Implementation issues on the design of current loops based on resonant regulators for isolated microgrids

Federico, de Bosio; Pastorelli, Michele; Antonio DeSouza Ribeiro, Luiz ; Freijedo Fernandez, Francisco Daniel; Guerrero, Josep M.

Published in:
Proceedings of 18th European Conference on Power Electronics and Applications (EPE'16 ECCE, Europe), 2016

DOI (link to publication from Publisher):
10.1109/EPE.2016.7695487

Publication date:
2016

Document Version
Early version, also known as pre-print

Implementation issues on the design of current loops based on resonant regulators for isolated microgrids

Federico de Bosio, Michele Pastorelli
Energy Department
Politecnico di Torino
Corso Duca degli Abruzzi, 24
10129 Torino, Italy
federico.debosio@polito.it
michele.pastorelli@polito.it

Luiz Antonio de Souza Ribeiro
Institute of Electrical Energy
Federal University of Maranhao
Av. Dos Portugueses, 1966
65072010 Sao Luis MA, Brazil
l.a.desouzaribeiro@ieee.org

Francisco Daniel Freijedo
Power Electronics Lab
École Polytechnique Fédérale de Lausanne
ELD 137, Station 11
1015 Lausanne, Vaud, Switzerland
francisco.freijedo@epfl.ch

Josep Maria Guerrero
Institute of Energy Technology
Aalborg University
Pontoppidanstraede, 101/45
9200 Aalborg, Denmark
joz@et.aau.dk
www.microgrids.et.aau.dk

Acknowledgements

This work was supported in part by the CNPq/Brazil, CEMAR, and Schneider Electric.

Keywords

«Current regulator», «Voltage Regulator», «Power Quality», «Microgrids».

Abstract

This paper analyzes the influence of state feedback coupling between the capacitor voltage and inductor current in voltage source inverters (VSI) operating in stand-alone microgrids. A decoupling technique is proposed as an effective measure to enhance the dynamics. Further implementation issues and control structures are also considered. Lab-scale experimental results prove the validity of the approaches.

Introduction

Voltage and current regulators play an important role in modern applications of power electronics, such as variable speed drives, active power filters, and microgrids [1]-[3]. The general power processor unit used in these applications is the Voltage Source Inverter (VSI) operating in current or voltage control mode depending on the application. The current loops are responsible for controlling torque in ac machines, harmonic compensation in active power filters and microgrids. Moreover, current and voltage regulation is needed in isolated microgrids. Hence, accurate control of current, voltage or both is required for the VSI to succeed in implementing the desired feature of each application. It is expected from any current or voltage regulator to [3],[4]: *i*) achieve zero steady-state error; *ii*) accurately track the commanded reference during transients; *iii*) have a bandwidth as widen as possible; and *iv*) mitigate low order harmonics.

Linear regulators suit very well for analysis with classical control theory. Among linear regulators the PI implemented in the stationary and synchronous reference frames [4],[5], and Proportional + Resonant (PR) [6] in the stationary reference frame are the most common regulators used in these applications. Due to the importance of these regulators, there has been substantial research activity in the subject throughout the years [7]-[10].

PR controllers avoid the rotations used in synchronous PI regulators and can be used directly in single-phase systems. In some applications, non-ideal PR is used to avoid implementation problems in low cost processors [6]. Another implementation, called complex vector PR was initially applied in sensorless ac drives [11]. It is derived from two complex vector PIs [12] and is implemented in the stationary reference frame. Independently of the PR controller used aspects of discretization, computation and PWM delays, and system couplings (when LC filters are used in the output of the VSI) are important issues that must be taken into account when designing these controllers [13].

This paper addresses the analysis and design of different current control implementations for VSI in isolated microgrids. Even though extensive research has been done in systems for grid connected applications, the isolated microgrid structure has not been previously discussed in depth. In such cases the coupling between the capacitor voltage and inductor current plays an important role in the performance of current regulators. The aim of this paper is to analyze the performance of current regulators with respect to: the effect of voltage coupling in the performance of these regulators; the effect of the computation and PWM delays in their design; the effect of discretization methods, and the main differences between the PR controllers.

System Description

The control of parallel-connected VSIs in isolated microgrids is based on droop control strategy that provides the voltage and frequency references for the inner loops [3]. In isolated microgrids the VSI operates in voltage mode where the capacitor voltage and inductor currents are the controlled states. The block diagram including three-phase three-legs inverter with its inner loops is presented in Fig. 1. The goal of the inner current loop is to track the commands from the outer voltage loop. Whenever the current regulator is unable to perform properly this goal the system performance degrades.

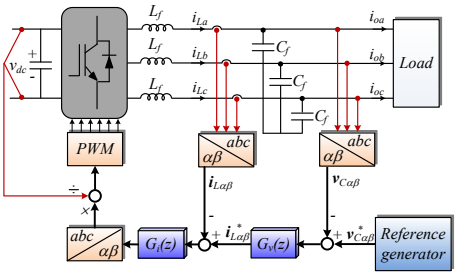

Fig. 1. Block diagram of a three phase VSI with voltage and current loops

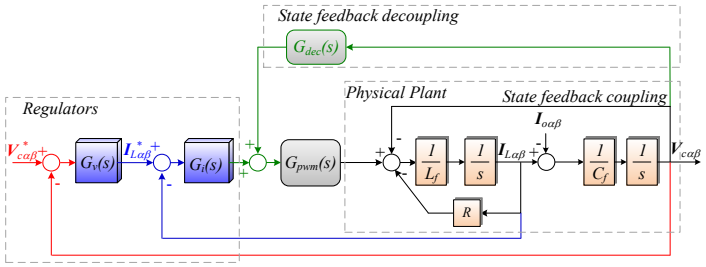

Fig. 2. Simplified state block diagram of the closed-loop system

The simplified control block diagram of the closed-loop system is shown in Fig. 2, where $\boldsymbol{V}^*_{c\alpha\beta}$ and $\boldsymbol{I}^*_{L\alpha\beta}$ are the reference voltage and current vectors and $\boldsymbol{I}_{o\alpha\beta}$ is the output current vector. $G_i(s)$ and $G_v(s)$ represent the current and voltage regulators transfer functions (TF), $G_{pwm}(s)$ is the TF related to computation and PWM delays, and $G_{dec}(s)$ is the TF related to the decoupling of state feedback cross-coupling.

Analysis and Design of Current Loop

In design cascaded or multiple loop systems as the one shown in Fig. 2 it is used serial tuning where the innermost current loop is designed first. The current regulators analyzed in this work are: i) proportional P; ii) ideal PR; iii) non-ideal PR, and iv) complex vector PR. The TF of each regulator are presented in Table I, where $\omega_o = 2\pi 50\, rad/s$ is the resonant frequency. First, the state feedback coupling effects in the application and delay modelling issues are analysed and a simple decoupling solution is proposed.

Capacitor voltage coupling and delay modelling issues

The basic assumption in ac drives and grid connected applications is to neglect the cross-coupling due to the capacitor voltage, i.e. the grid voltage or back-emf can be treated as a disturbance to the current loop. The regulator proportional gain is selected to achieve the desired bandwidth (f_{bw}), which should be much faster than the outer loops [14]. For the design of the regulator bandwidth, another assumption is to neglect the computation and PWM delays. However, the error introduced by this assumption can be very large depending on the delay ($G_{PWM}(s) = e^{-T_d s}$), its approximation used in the design, and on the chosen bandwidth. A first order Padé approximation for it is the common choice. There are at least two different ways to approximate the delay: 1) $e^{-T_d s} \cong 1/(1 + T_d s)$; 2) $e^{-T_d s} \cong [1 - (T_d/2)s]/[1 + (T_d/2)s]$. It can be seen that the second expression preserves the magnitude, and for frequencies until $0.1\mathrm{f_s}$ the phase difference is negligible. Therefore, it is more appropriate to be used to design the regulator. Furthermore, the non-minimum phase zero presented is useful to understand how the system can become unstable when the regulator gain increases [15]. For the value of the delay used in this application ($T_d = 1.5T_s$), and the bandwidth chosen for the inner loop ($f_{bw} = 1\ kHz$), the gain difference neglecting the delay model or including it is more than 50%, which proves the importance of its consideration in the tuning process when the system bandwidth approaches 10% of the switching frequency ($f_s = 1/T_s$).

Table I. Inner Current Loop $G_i(s)$

Non-ideal PR controller	Ideal PR controller	Complex vector PR controller
$k_{pI} + \frac{2\omega_c k_{iI} s}{s^2 + 2\omega_c s + (h\omega_o)^2}$	$k_{pI} + \frac{k_{iI} s}{s^2 + (h\omega_o)^2}$	$\frac{k_{pI} s^2 + k_{iI} s}{s^2 + (h\omega_o)^2}$

Table II. System parameters

Parameter	Value
Switching frequency	$f_s = 10\ kHz$
Filter inductance	$L_f = 1.8\ mH$
Filter capacitor	$C_f = 27\ \mu F$
Inductor ESR	$R = 0.1\ \Omega$
Rated load	$R_l = 68\ \Omega$

Table III. Control Parameters

Parameter	Value
Proportional gain	$k_{pI} = 6.42$
Integral gain	$k_{iI} = 311$
Damping term	$\omega_c = 5\ rad/s$

Because of the cross-coupling between the capacitor voltage and inductor current (see Fig. 2), the usual assumption in the design stage that the controlled states are decoupled does not hold true anymore. Fig. 3 shows the root locus (RL) for the inner current loop by considering the delay model $G_{PWM}(s) = [1 - (T_d/2)s]/[1 + (T_d/2)s]$.

The system and control parameters used in the simulation and experimental results are presented in Table II and Table III, respectively. Due to the capacitor coupling the dominant open loop poles are imaginary. As a result, the closed loop system has low damping no matter the tuned gain. For the desired bandwidth of 1 kHz ($k_{pi} = 5.62$), the closed loop poles and their features are presented in detail. Furthermore, this RL shows that due to the right half plane zero (non-minimal phase zero) the system can become unstable for certain gain values. This behaviour cannot be predicted when $G_{PWM}(s) = 1/[1 + T_d s]$ is used as approximation

Ideally, if it is possible to exact decouple the controlled states (cancel the cross-coupling) as shown in Fig. 2, the inner current loop is not affected anymore by the capacitor voltage. The open loop transfer function used to analyse and design the current loop is $OL(s) = k_{pI} G_{PWM}(s)/(Ls + R)$. The correspondent RL is shown in Fig. 4. As can be seen, due to the cross-coupling decoupling the open loop poles are real. Therefore, the tuning is much easier and the resulted closed loop poles (showed in the highlighted area) for the same bandwidth of 1 kHz present a damping much higher than for the case without decoupling**.** Furthermore, the system will be stable for values of $k_{pI} < (2L + RT_d)/T_d$. For the plant values, $k_{pI} < 24.1$ results in a stable system.

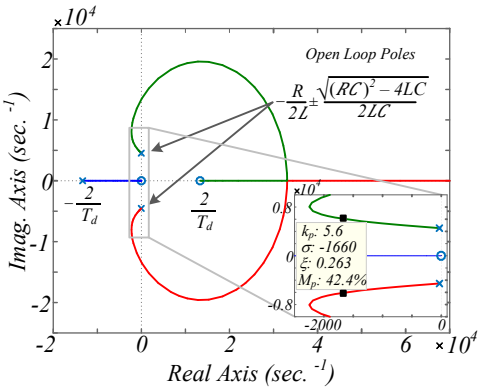

Fig. 3. Root locus for the inner current loop with P regulator and without voltage decoupling: x – open loop poles; ■ closed loop poles for $k_{pI} = 5.61$; o – zeros; $G_{PWM}(s) = [1 - (T_d/2)s]/[1 + (T_d/2)s]$

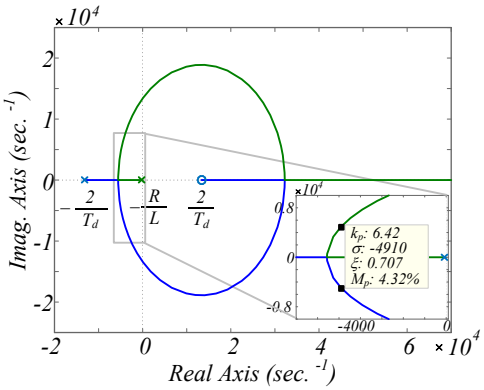

Fig. 4. Root locus for the inner current loop with P regulator and voltage decoupling: x – open loop poles; ■ closed loop poles for $k_{pI} = 6.42$; o – zeros; $G_{PWM}(s) = [1 - (T_d/2)s]/[1 + (T_d/2)s]$

The command tracking frequency responses (FR) for the inner current loop with and without voltage decoupling are presented in Fig. 5. For the case without voltage decoupling the FR is dependent on the load. The arrow in the FR indicates decreasing in load from rated to no-load condition. It is difficult to assess the bandwidth of the system when voltage decoupling is not performed. This is because the gain at low frequencies is changing. The main outcome is that, independent of the load level, at the desired fundamental frequency (50 Hz) the gain is very low implying a very high steady-state error if a proportional regulator is used. However, if voltage decoupling is performed the frequency response is independent of the load and the steady-state error is small even with a proportional regulator. For this last case it can be seen that the system bandwidth is approximately 1 kHz, as designed.

Main controller structures

By observing the FR of the inner current loop without voltage decoupling it is clear that a proportional regulator cannot be used due to the resulted very high steady-state error. That is why in some research work the authors suggest to use resonant regulators for this loop [3].

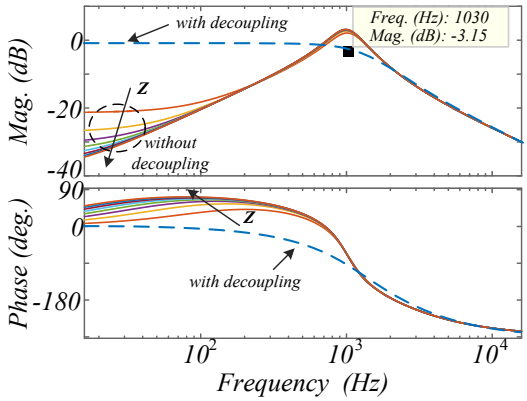

Fig. 5. Closed loop FR for the inner current loop with P regulator and with and without voltage decoupling – arrows indicate decreasing in load (from rated load until no-load); $G_{PWM}(s) = [1 - (T_d/2)s]/[1 + (T_d/2)s]$

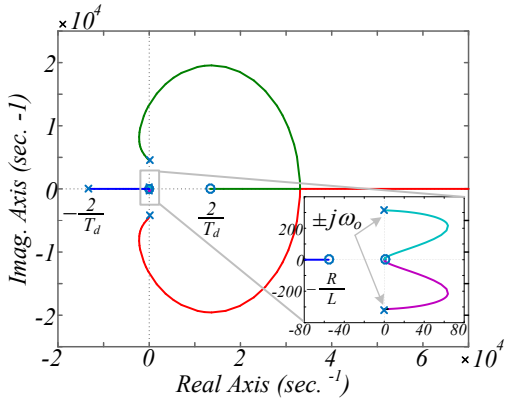

Fig. 6. Root locus of the inner current loop with complex vector PR regulator and without voltage decoupling: x – open loop poles; o – zeros; $k_{iI}/k_{pI} = R/L$; $G_{PWM}(s) = [1 - (T_d/2)s]/[1 + (T_d/2)s]$

However, if among the resonant regulators in Table I the complex vector PR is used without voltage decoupling the system is unstable, independently of the regulator gains. This can be observed on the RL showed in Fig. 6. For this case the design of the regulator zero was made to cancel the plant pole

($k_{iI}/k_{pI} = R/L$) as reported in Table III. Nevertheless, the instability is independent of the zero location.

The frequency response (FR) for each regulator was analysed for different values of the integral gain k_{iI} in the range 11-511, around the value designed to cancel the dominant pole of the plant. Fig. 7(a) and Fig. 7(b) show the closed loop FR of the current loop only of the system in Fig. 2 with voltage decoupling, using non-ideal and ideal PR as current regulator respectively. With reference to non-ideal PR [see Fig. 7(a)], it can be observed that:

1) the ability to reduce the steady-state error at the desired resonant frequency (50 Hz) is dependent on the integral gain (k_{iI}), the smaller its value the bigger will be the error at this frequency;
2) changes in the resonant frequency can have a significant impact on the steady-state error;
3) the results become worse as the bandwidth of the controller decreases.

A similar FR is obtained when the ideal PR is used for the inner current loop [see Fig. 7(b)]. Similar conclusions as for non-ideal PR can be derived, but small changes in frequency can result in much higher steady-state error at the resonant frequency.

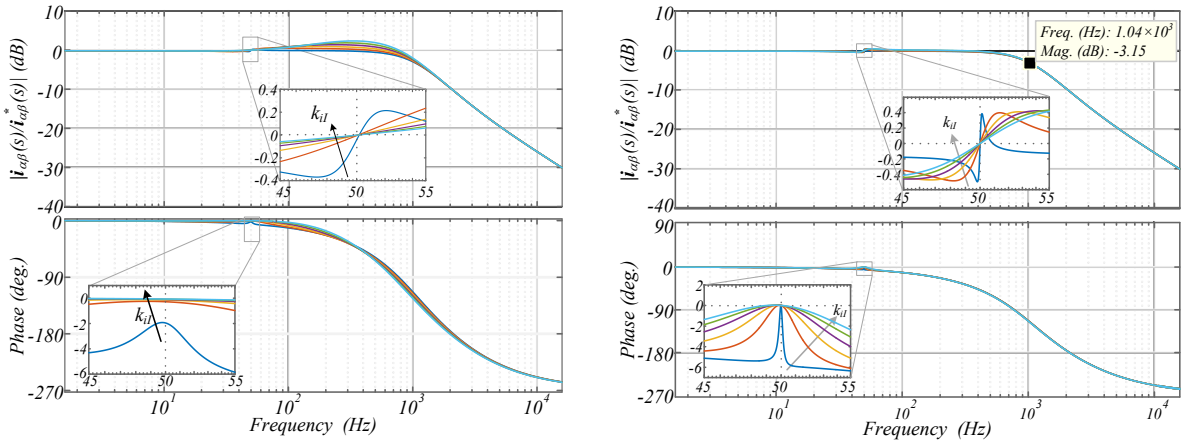

(a) (b)

Fig. 7. Closed loop FR of the inner current loop with voltage decoupling and $k_{pI} = 5.61$; $k_{iI} = 11 - 511$ (arrows indicate increasing of k_{iI}): (a) non-ideal PR regulator; (b) ideal PR regulator

If voltage decoupling is performed, as proposed in this work, the complex vector PR can be used and the system can take advantage of its good properties.

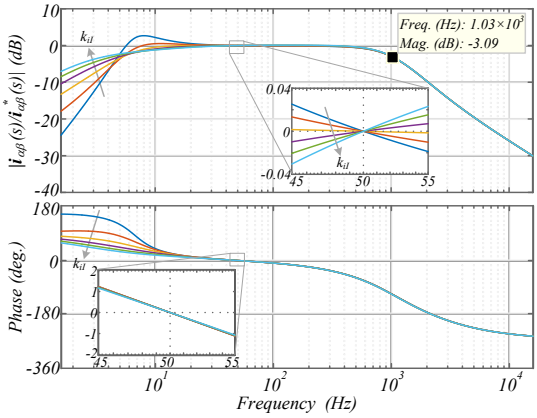

Fig. 8. Closed loop FR of the inner current loop with ideal PR regulator and without voltage decoupling: $k_{pI} = 5.61$; $k_{iI} = 11 - 511$ (arrows indicate increasing of k_{iI})

The load does not disturb the current regulator anymore, so that the errors are extremely low around the resonant frequency, as can be seen in Fig. 8. Furthermore, the closed loop anomalous peak that appears in ideal PR does not show up anymore. Comparing this controller with the others

analyzed in this paper it can be stated that it is the one that presents the lowest sensitivity to frequency variations around the resonant frequency, independently of the integral gains used [16]. Therefore, complex vector PR is the most indicated for use in applications where the resonant frequency changes as in droop controlled microgrids [17].

Effects of discretization methods

In real time applications, in general all the regulators are implemented in the discrete time domain. A common way of implementing PR regulators is based on the structure with two cascaded integrators, using forward and backward Euler as discretization methods [18]. The implementations in the s-domain and z-domain are shown for ideal PR in Fig. 9(a) and Fig. 9(b) respectively.

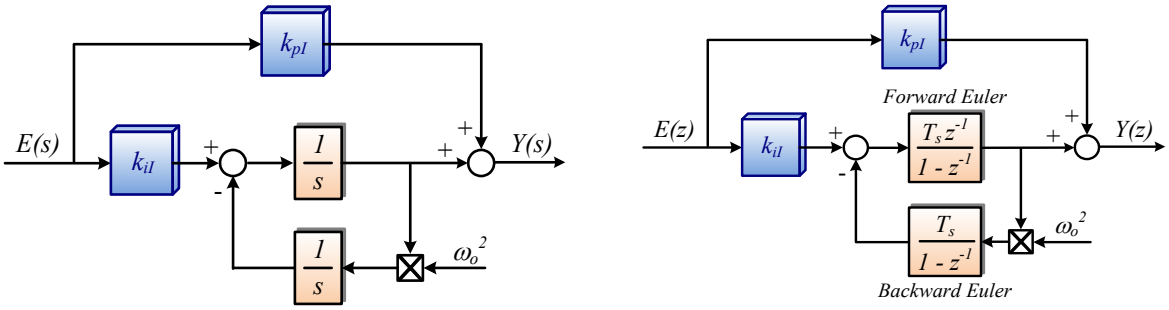

Fig. 9. Implementation of ideal PR with the two integrator structure: (a) in the s-domain (b) in the z-domain using Forward and Backward Euler as discretization methods

Several possibilities can be used for the method that discretizes the PR regulators, e.g. Impulse Invariant, Tustin with frequency prewarping. The use of these methods implies the discretization of the resonant part of the regulator. For the case of the ideal PR, the transfer function for any harmonic of the fundamental resonant frequency is

$$G_i(s) = \frac{Y(s)}{E(s)} = k_{pI} + k_{iI,h}\frac{s}{s^2 + h^2\omega_o^2} \rightarrow G_i(s) = k_{pI} + k_{iI,h}R_{1,h}(s), \quad (1)$$

where h is the number that represents each harmonic of the fundamental resonant frequency (ω_o). The discrete version of $R_{1,h}(s)$ using Impulse Invariant and Tustin with frequency prewarping is presented in Table IV.

Table IV. Z-Domain transfer functions of $R_{1,h}(s)$ using Impulse Invariant and Tustin with Prewarping methods

Impulse Invariant	Tustin with Frequency Prewarping
$R_{1,h}(z) = T_s\frac{1 - z^{-1}\cos(h\omega_o T_s)}{1 - 2z^{-1}\cos(h\omega_o T_{sw}) + z^{-2}}$	$R_{1,h}(z) = \frac{\sin(h\omega_o T_s)}{2h\omega_o}\frac{1 - z^{-2}}{1 - 2z^{-1}\cos(h\omega_o T_s) + z^{-2}}$

To analyze the effect of the discretization methods on the close loop FR, the system close loop FR in s-domain was compared to the close loop FR in z-domain. For the z-domain, the transfer functions of the regulators were discretized using the Forward and backward Euler, the Impulse Invariant and Tustin with prewarping methods.

At low and fundamental frequencies there is no difference between the continuous and discrete time FR, no matter the discretization method used. However, as the frequency increases the discrete time FR using the structure with two integrators does not represents adequately the continuous time behavior [see Fig. 10(a)]. There is a shift in the frequency response around the resonant frequency and the regulator does not produce anymore the desired feature of zero steady-state error (0 dB, 0^o) at the designed resonant frequency.

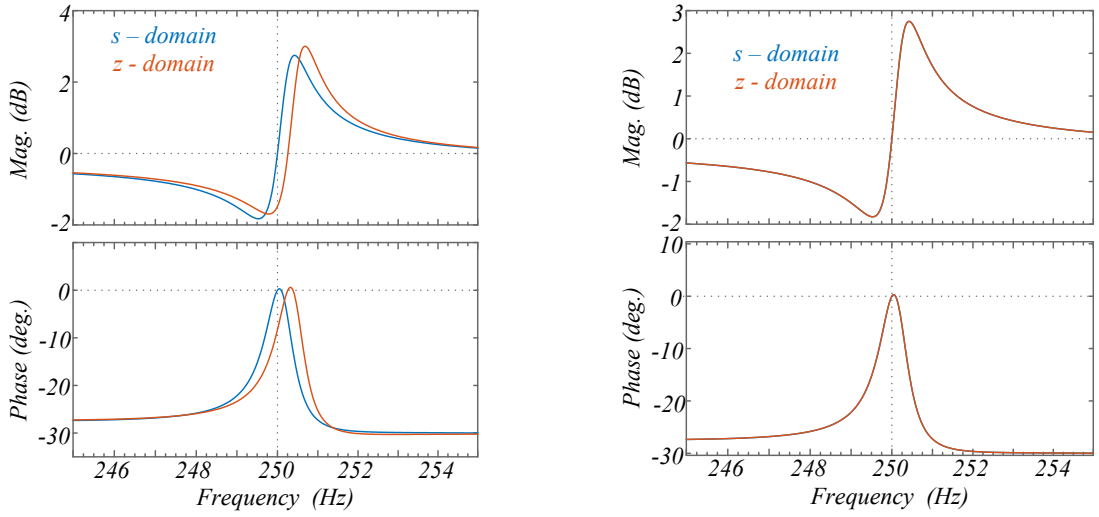

Fig. 10. Comparison of the continuous and discrete time closed loop FR of the inner current loop with ideal PR regulator and with voltage decoupling at 5th harmonic of the fundamental frequency: (a) structure with 2 integrators - Forward and backward Euler method; (b) Impulse Invariant method.

Furthermore, the bigger the resonant frequency the bigger will be the shift in the FR, as can be seen in Fig. 11(a). However, using other discretization methods, such as Impulse Invariant, a better match between the continuous to the discrete time domain is achieved [9], as shown in Fig. 10(b) and Fig. 11(b). Although it is not shown in the figures the discretization using Tustin with frequency prewarping produces similar results as the Impulse Invariant method. Similar results apply for the other PR regulators investigated, i.e. non-ideal PR and Complex Vector PR.

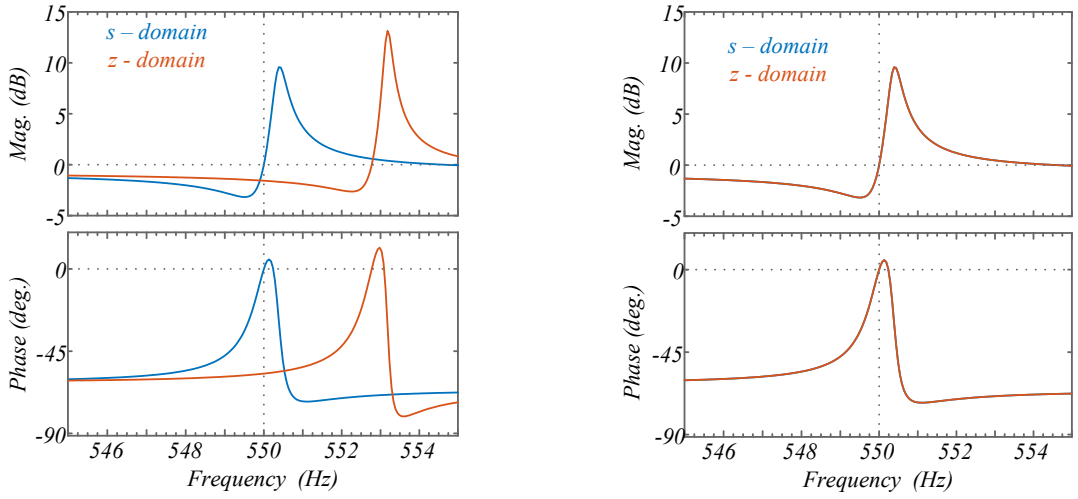

Fig. 11. Comparison of the continuous and discrete time closed loop FR of the inner current loop with ideal PR regulator and with voltage decoupling at 11th harmonic of the fundamental frequency: (a) structure with 2 integrators - Forward and backward Euler method; (b) Impulse Invariant method.

Experimental Results

The power system of Fig. 1 was tested to check the analysis presented. For this purpose, a low scale test-bed has been built using a Danfoss 2.2 kW converter, driven by a dSpace DS1006 platform. The measured variables are sensed via LEM current and voltage transducers and sent to the 16-bit resolution high-speed A/D board DS2004 for digitizing the input signals at high sample rates. The filter parameters and operational information are presented in Table II.

Fig. 12 and Fig. 13 show the results for a 5th harmonic reference current tracking using two different discretization methods for ideal PR. If the structure with two integrators with forward and backward Euler discretization methods is used (Fig. 12), the controller is not able to achieve zero steady-state error, as expected from the previous FR analysis. However, if ideal PR is implemented without splitting the resonant term in two integrators, zero steady-state error can be achieved (Fig. 13).

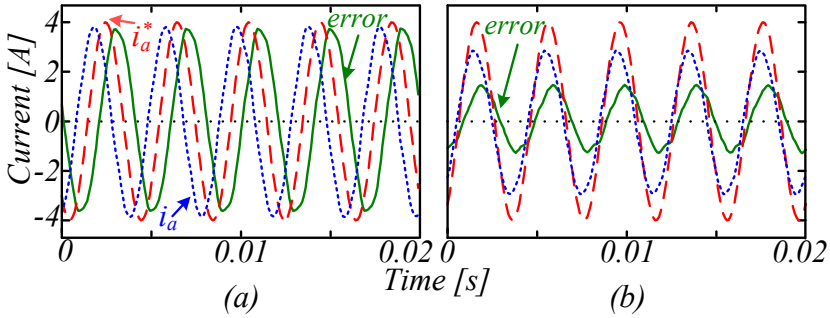

Fig. 12. Structure with two integrators: steady-state currents and error for ideal PR 5th harmonic reference tracking: (a) without voltage decoupling; (b) with voltage decoupling

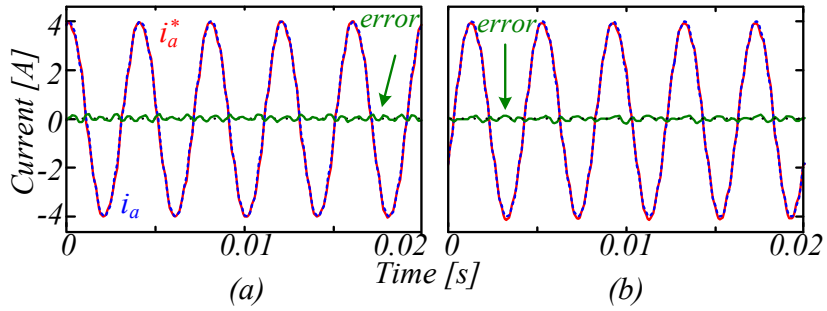

Fig. 13. Impulse Invariant discretization method: steady-state currents and error for ideal PR 5th harmonic reference tracking: (a) without voltage decoupling; (b) with voltage decoupling

As expected from the FR analysis all the three controllers achieve approximately zero steady-state error when designed to have exactly the same resonant frequency as the one of the reference current, implemented with the correct discretization method, and for high k_{iI} as in Table III. To analyze the sensitivity of the PR regulators to frequency variations the reference current frequency was changed to 49 Hz, while the regulator design was kept at 50 Hz. Fig. 14 shows the steady-state currents and error in α-axis for ideal PR regulator without and with voltage decoupling with the gains provided in Table III. Without voltage decoupling the current error is mainly due to the difference in phase between the reference i_α^* and real current i_α. The effect of voltage decoupling has a significant impact on the system performance, reducing the error. The same conclusion can be drawn for the case of the non-ideal PR, except that the error is smaller (see Fig. 15). Comparing Fig. 14 and Fig. 15, it seems that the non-ideal PR has better performance than the ideal one.

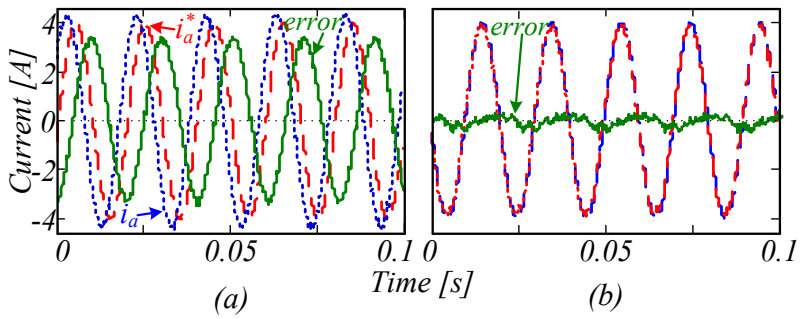

Fig. 14. Steady-state currents and error for ideal PR (α-axis): (a) without voltage decoupling; (b) with voltage decoupling - $f_{ref} = 49\ Hz$, $k_{iI} = 311$

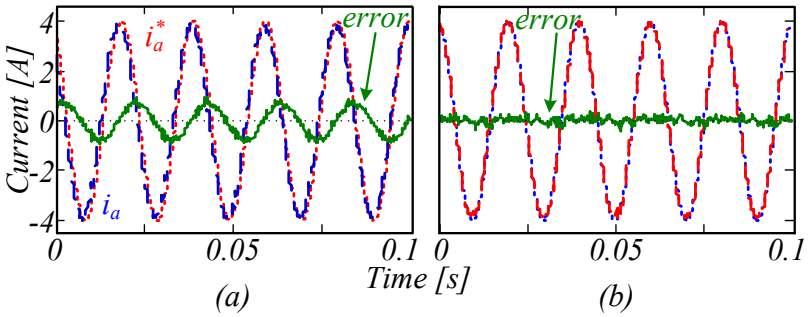

Fig. 15. Steady-state currents and error for non-ideal PR (α-axis): (a) without voltage decoupling; (b) with voltage decoupling - $f_{ref} = 49\ Hz$, $k_{il} = 311$

However, as the integral gain is reduced to lower values (see Fig. 16) the performance of non-ideal PR to frequency variation degrades.

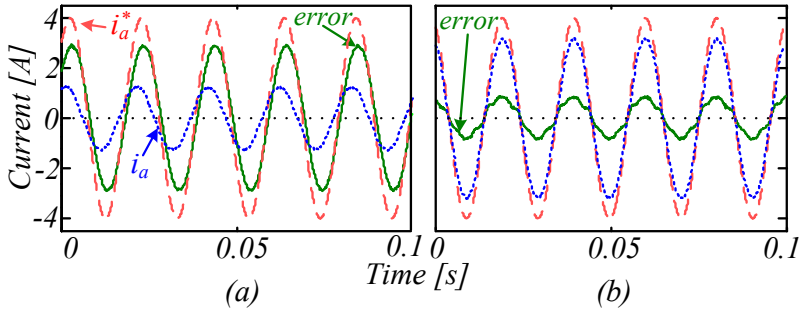

Fig. 16. Steady-state currents and error for non-ideal PR (α-axis): (a) without voltage decoupling; (b) with voltage decoupling - $f_{ref} = 49\ Hz$, $k_{il} = 11$

On the other hand, complex vector PR is still able to achieve zero steady-state error regardless the integral gain value (see Fig. 17). Thus, the complex vector PR should be preferred when there are frequency variations, as is the case in droop controlled microgrids. Furthermore, its performance is less sensitive to the design of the integral gain.

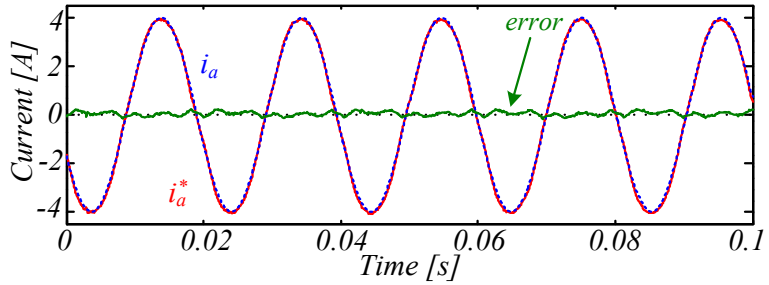

Fig. 17. Steady-state currents and error for Complex vector PR (α-axis) with voltage decoupling - $f_{ref} = 49\ Hz$, $k_{il} = 11$

Conclusion

In this paper, an analysis and design of the inner current loop for power converters in islanding microgrid applications based on PR regulators has been carried out. The benefits of applying capacitor voltage decoupling are motivated by the lower steady-state error. Complex vector PR controller, which is stable only if voltage decoupling is performed, shows the lowest sensitivity to integral gain and frequency deviations, thus can be preferred in microgrid applications. The discretization method plays an important role in the performance of the resonant regulators. If the wrong discretization method is used the PR regulator does not produce the desired effect, in particular as harmonic compensators are implemented.

References

[1] D. G. Holmes, T. A. Lipo, B. P. McGrath, and W. Y. Kong, "Optimized Design of Stationary Frame Three Phase AC Current Regulators," *IEEE Trans. Power Electron.,* vol. 24, no. 11, pp. 2417-2426, 2009.

[2] C. Lascu, L. Asiminoaei, I. Boldea, and F. Blaabjerg, "High Performance Current Controller for Selective Harmonic Compensation in Active Power Filters," *IEEE Trans. Power Electron.,* vol. 22, no. 5, pp. 1826-1835, 2007.

[3] J. C. Vasquez, J. M. Guerrero, M. Savaghebi, J. Eloy-Garcia, and R. Teodorescu, "Modeling, Analysis, and Design of Stationary-Reference-Frame Droop-Controlled Parallel Three-Phase Voltage Source Inverters," *IEEE Trans. Ind. Electron.,* vol. 60, no. 4, pp. 1271-1280, 2013.

[4] T. M. Rowan and R. J. Kerkman, "A New Synchronous Current Regulator and an Analysis of Current-Regulated PWM Inverters," *IEEE Trans. Ind. Appl.,* vol. IA-22, no. 4, pp. 678-690, 1986.

[5] B. P. McGrath, S. G. Parker, and D. G. Holmes, "High Performance Stationary Frame AC Current Regulation Incorporating Transport Delay Compensation," *EPE Journal,* vol. 22, no. 4, pp. 17-24, 2012.

[6] D. N. Zmood and D. G. Holmes, "Stationary frame current regulation of PWM inverters with zero steady-state error," *IEEE Trans. Power Electron.,* vol. 18, no. 3, pp. 814-822, 2003.

[7] K. Hongrae, M. W. Degner, J. M. Guerrero, F. Briz, and R. D. Lorenz, "Discrete-Time Current Regulator Design for AC Machine Drives," *IEEE Trans. Ind. Appl.,* vol. 46, no. 4, pp. 1425-1435, 2010.

[8] J. Holtz, Q. Juntao, J. Pontt, J. Rodriguez, P. Newman, and H. Miranda, "Design of fast and robust current regulators for high-power drives based on complex state variables," *IEEE Trans. Ind. Appl.,* vol. 40, no. 5, pp. 1388-1397, 2004.

[9] A. G. Yepes, F. D. Freijedo, J. Doval-Gandoy, Lo, x, O. pez*, et al.*, "Effects of Discretization Methods on the Performance of Resonant Controllers," *IEEE Trans. Power Electron.,* vol. 25, no. 7, pp. 1692-1712, 2010.

[10] A. G. Yepes, F. D. Freijedo, O. Lopez, and J. Doval-Gandoy, "Analysis and Design of Resonant Current Controllers for Voltage-Source Converters by Means of Nyquist Diagrams and Sensitivity Function," *IEEE Trans. Ind. Electron.,* vol. 58, no. 11, pp. 5231-5250, 2011.

[11] L. A. de S. Ribeiro, M. W. Degner, F. Briz, and R. D. Lorenz, "Comparison of carrier signal voltage and current injection for the estimation of flux angle or rotor position," in *Industry Applications IEEE Conference, Thirty-Third IAS Annual Meeting*, 1998, pp. 452-459, vol 1.

[12] F. Briz, M. W. Degner, and R. D. Lorenz, "Analysis and design of current regulators using complex vectors," *IEEE Trans. Ind. Appl.,* vol. 36, no. 3, pp. 817-825, 2000.

[13] F. de Bosio, L. A. de S. Ribeiro, F. D. Freijedo, M. Pastorelli, and J. M. Guerrero, " Effect of state feedback coupling and system delays on the transient performance of stand-alone VSI with LC output filter," *IEEE Trans. Ind. Electron.*, Early Access, 2016.

[14] K. J. Aström and T. Hägglung, PID Controllers: Theory, Designing, and Tuning, 2nd ed., Research Triangle Park, NC, USA: Instrument Society of America, 1995. 2006.

[15] F. D. Freijedo, A. Vidal, A. G. Yepes, J. M. Guerrero, O. Lopez, J. Malvar, and Jesús Doval-Gandoy, "Tuning of Synchronous-Frame PI Current Controllers in Grid-Connected Converters Operating at a Low Sampling Rate by MIMO Root Locus," *IEEE Trans. Ind. Electron.,* vol. 62, no. 8, pp. 5006-5017, 2015.

[16] F. de Bosio, L. A. de S. Ribeiro, M. S. Lima, F. Freijedo, J. M. Guerrero, and M. Pastorelli, "Current control loop design and analysis based on resonant regulators for microgrid applications," in *IEEE Conf. Rec. IECON*, Yokohama, Japan, 2015, pp. 5322 - 5327.

[17] J. M. Guerrero, M. Chandorkar, T.-L. Lee, and P. C. Loh, "Advanced Control Architectures for Intelligent Microgrids—Part I: Decentralized and Hierarchical Control," *IEEE Trans. Ind. Electron.,* vol. 60, no. 4, pp. 1254 - 1261, 2013.

[18] R. Teodorescu, F. Blaabjerg, M. Liserre, and P. C. Loh, "Proportional-resonant controllers and filters for grid-connected voltage-source converters," in *IEEE Conf. Rec Electric Power Applications.,* vol. 153, no. 5, pp. 750-762, 2006.